Applied Catalysis B: Environmental 338 (2023) 123056

Contents lists available at ScienceDirect

Applied Catalysis B: Environmental

journal homepage: www.elsevier.com/locate/apcatb

Boosting efficient C-N bonding toward photoelectrocatalytic urea synthesis from CO_2 and nitrate via close Cu/Ti bimetallic sites

Jingui Zheng [a], Shaohan Xu [a], Jie Sun [a], Jinxing Zhang [a], Lingzhi Sun [a], Xun Pan [a], Lina Li [b], Guohua Zhao [a,*]

[a] Shanghai Key Lab of Chemical Assessment and Sustainability, School of Chemical Science and Engineering, Tongji University, Shanghai 200092, China
[b] Shanghai Synchrotron Radiation Facility, Shanghai Advanced Research Institute, Shanghai 201800, China

ARTICLE INFO

Keywords:
Urea synthesis
CO_2 and nitrate co-reduction
C-N bonding
Cu/Ti bimetallic sites
Photoelectrocatalysis

ABSTRACT

The urea synthesis is limited by inefficiently C-N bonding from CO_2 and nitrate. Here, we engineered dual metal Cu and Ti active sites with short distance by single atom Cu anchored on TiO_2, which is conducive to C-N bonding for photoelectrocatalytic urea synthesis with CO_2 and nitrate, achieving record-highest urea Faradic efficiency of 68%. The Cu site efficiently catalyzed reduction of CO_2 to *CO, and adjacent Ti site catalyzed reduction of nitrate to $*NH_2$ intermediate on SAC Cu-TiO_2. The close Cu and Ti sites shorten distance between *CO and $*NH_2$ intermediate for coupling, which is conducive to C-N bonding for photoelectrocatalytic synthesizing urea. DFT and in-situ FT-IR spectroscopy suggested that compared with their parallel competing reactions of $*NH_2$ and *CO intermediates, coupling of *CO and $*NH_2$ at close Cu and Ti sites had a lower energy barrier on SAC Cu-TiO_2, which is an important reason for efficient synthesis of urea.

1. Introduction

As a representative greenhouse gas and water pollutants, the CO_2 and nitrate wastewater have caused serious environmental problems, threatening the survival and development of human beings [1–4]. Converting them into high-value chemicals is considered as a promising way to reduce environmental pollution and realize the utilization of waste resources [5–7]. A new waste management strategy that kills two birds with one stone is proposed to simultaneously convert CO_2 and nitrate into high value-added urea by C-N bonding ($2NO_3^- + CO_2 + 18H^+ + 16e^- \rightarrow NH_2CONH_2 + 7H_2O$) [8–10]. However, how to promote the C-N bonding has always been a challenge for urea synthesis in the process of CO_2 and nitrate reduction reaction.

Aiming at efficient synthesis of urea from greenhouse gas CO_2 and nitrate wastewater, some researchers promoted C-N bonding by accelerating the generation of specific reaction intermediates of CO_2 and nitrate for coupling by electrochemical ways. Zhang's group suggested that the urea formation was accelerated by promoting the formation of $*NH_2$ and *COOH intermediates in the process of electrochemical reduction of nitrite and CO_2 on oxygen-rich vacancy ZnO porous nanosheets [11]. However, it is hard to achieve the simultaneously catalytic reduction of two reactants CO_2 and nitrate at a single active site [12,13]. Therefore, constructing bimetallic active sites is a feasible method to simultaneously catalyze the reduction of CO_2 and nitrate to C-N bonding. Shao's group showed that CO_2 reduction to *CO intermediate and NO_2^- reduction to $*NH_2$ intermediate can be promoted by cooperation of metals between Te and Pd [14]. Then, efficient C-N bonding between *CO and $*NH_2$ coupling takes place to form urea with a Faradaic efficiency (FE) of 8.92%. However, due to the long distance between the coupling reaction intermediates generated at the bimetallic sites in the alloy, it is difficult to achieve efficient coupling between CO_2 and nitrate reduction intermediates.

Hence, structuring bimetallic active site with short distance for the simultaneous catalytic co-reduction of CO_2 and nitrate is conducive to the C-N coupling between reduction intermediate of CO_2 and nitrate for urea synthesis. Wang's group constructed a Fe Ni bimetallic single atom catalyst with a short distance of 2.5 Å between bimetallic active sites, which can simultaneously catalyze the reduction of CO_2 and NO_3^- respectively to synthesize urea [15]. The Faradaic efficiency of CO_2 reduction to CO and nitrate reduction to NH_3 on Ni Fe bimetallic single atom catalyst were 73.3% and 77.6%, respectively, but the Faradaic efficiency of urea synthesis was only 17.8% by C-N bonding from CO_2 and nitrate. The reason may be that the reduction intermediates of CO_2 and nitrate may not undergo selective C-N coupling, but their parallel

* Corresponding author.
E-mail address: g.zhao@tongji.edu.cn (G. Zhao).

https://doi.org/10.1016/j.apcatb.2023.123056
Received 17 April 2023; Received in revised form 18 June 2023; Accepted 27 June 2023
Available online 28 June 2023

competing reduction reactions occur. The desorption, hydrogenation and dimerization of reduction reaction intermediates of CO_2 and nitrate are important factors restricting the efficient synthesis of urea. When CO_2 is reduced to form the *CO intermediate, which is favorable for C-N bonding, the *CO intermediate is easily desorbed from the surface of the catalyst to generate CO [16–18], extremely limiting its subsequent coupling reaction with $*NH_2$. Furthermore, the *CO intermediate may continue to be hydrogenated to form *HCO, which can undergo multi-step reduction reaction to form C1 products such as methane [19–21], methanol [22], formic acid [23] and so on. In addition, the *CO intermediate may also dimerize to form *OCCO intermediates, which may be subsequently reduced to C_2 products such as ethanol [24,25], acetylene [26], ethylene [27–29]. Similarly, when nitrate is reduced to an $*NH_2$ intermediate, the $*NH_2$ intermediate may continue to be hydrogenated to form NH_3 or coupled to form N_2H_4 [30,31]. Therefore, the main challenge of C-N bonding for urea synthesis can be ascribed that CO_2 and nitrate can be efficiently reduced to specific reaction intermediates, which can be selective C-N bonding rather than parallel competing reactions of CO_2/NO_3^- reduction intermediates on catalyst.

Therefore, we engineered dual metal Cu and Ti active sites with a short distance by single atom Cu anchored on TiO_2 toward photoelectrocatalytic urea synthesis from CO_2 and nitrate. Cu and Ti dual active sites can efficiently catalyze the reduction of CO_2 to *CO and reduction of nitrate to $*NH_2$ intermediates, respectively. The relatively short distance of the Ti and Cu double site on SAC Cu-TiO_2 is 2 Å, which is conducive to the coupling of the two reaction intermediates *CO and $*NH_2$ to formation urea via C-N bonding by strong nucleophilic attack of $*NH_2$. Density functional theory (DFT) calculations verified that compared with parallel competing reactions of *CO and $*NH_2$ such as *CO hydrogenation, $*NH_2$ hydrogenation and its dimerization, the coupling of *CO and $*NH_2$ has a lower energy barrier on dual metal active sites with short distance by single atom Cu anchored on TiO_2. Therefore, we achieved the highest Faradaic efficiency for urea synthesis on SAC Cu-TiO_2 so far reported in the literature. The Faradic efficiency of urea synthesis by $*NH_2$ and *CO coupling is as high as 68% on SAC Cu-TiO_2 under the condition of light and − 0.5 V, which is 1.58 times higher than that of single metal active site on TiO_2. In addition, pathway of $*NH_2$ and *CO coupling for urea synthesis has faster reaction kinetics, while its urea yield is 2.2 times that of $*NH_2$ and $*CO_2$ direct coupling at − 0.5 V. This work provides new insight for the comprehensive treatment of CO_2 and nitrate pollutants, and also provide vital guidance for the synthesis of long-chain high value-added chemicals through efficient C-N bonding.

2. Experimental section

2.1. Preparation of photoelectrocatalysts

2.1.1. Synthesis of TiO_2 nanosheets

TiO_2 was prepared as a supported catalyst by a conventional hydrothermal method [32]. Hydrofluoric acid (HF, 3 mL) was slowly added to 25 mL of tetrabutyl titanate, and then stirred for 5 min to form a uniform mixture solution. The obtained mixture was transferred to a 50 mL Teflon-lined stainless steel autoclave and held at 180 °C for 24 h. After the hydrothermal reaction, the precipitate was carefully collected and washed several times with deionized water and absolute ethanol, respectively. The precipitates were dissolved in NaOH aqueous solution (0.1 M) and stirred for 7 h to remove the fluorine species to obtain pure TiO_2 nanosheets.

2.1.2. Synthesis of SAC Cu-TiO_2 photoelectrocatalyst

According to previous literature methods, the atomic dispersion of Cu species anchored on TiO_2 nanosheets was achieved by a precipitation method [33]. The prepared TiO_2 nanosheets (40 mg) were dispersed in 40 mL of NaOH aqueous solution (0.25 M). At room temperature, accompanied with stirring, the 650 μ L of Cu $(NO_3)_2$ aqueous solution (0.0077 M) was added to the solution prepared above. After stirring for 6 h, the precipitate was washed several times with deionized water until the pH of solution was 7. Finally, the washed sediment was dried at 353 K for 12 h to obtain SAC Cu anchored TiO_2 catalyst. The Cu content of the SAC Cu-TiO_2 catalyst we prepared was analyzed by ICP-MS, it was found that the Cu content was 0.58 wt.%. For comparison, Cu nanoparticles loaded TiO_2 (Cu amount: 0.58 wt.%) (Cu NPs-TiO_2) was gained by mechanically lapping of commercial Cu metal nanoparticles and prepared TiO_2.

2.2. Material characterization

The crystalline structures of the catalysts were tested by X-ray diffraction (XRD, D8 Focus X-ray diffractometer, Bruker, Germany), and the chemical states of catalysts were determined by X-ray photoelectron spectroscopy (XPS, AXIS Ultra DLD). Extended X-ray absorption fine structure (EXAFS) of SAC Cu-TiO_2 was detected on the 14b beamline at the Shanghai Synchrotron Radiation Facility (SSRF). The yields of gaseous products of CO_2 reduction were analyzed by online gas chromatography (GC-2014 C, Shimadzu). A 300 W xenon lamp (PLS-SXE300D, Beijing Perfect Light Technology Co., Ltd.) with a long-pass filter was used as the light source. The in-situ photoelectrochemical Fourier transform infrared spectroscopy (FTIR, Nicolet 8700, Thermo Fisher Scientific Inc., USA) was used to detect the reaction intermediates of the conversion of CO_2 and nitrate to urea at different potentials and light.

2.3. Photoelectrochemical measurements

To prepare the photoelectrocathode, 2 mg of sample, 350 μL of ethanol and 50 μL of Nafion (5%) solution were added to 600 μL of deionized water and sonicated for 1 h to mix uniformly. Then, carbon paper (1 cm × 2 cm) was coated with 500 μL of the as-prepared ink. The prepared working electrode was then dried at 60 ℃ for 3 h. The photoelectrocatalytic reduction of nitrate and CO_2 to urea was carried out in a H-cell reactor with 4.5 mL of electrolyte. The prepared electrode and Pt sheet were respectively used as the working electrode and counter electrode, and a saturated calomel electrode was used as the reference electrode.

2.4. In-situ infrared spectroscopic measurements

The in-situ photoelectrochemical infrared spectra were recorded on an infrared spectrometer (Nicolet 8700, Thermo Fisher Scientific Inc., USA). The applied potential was adjusted by a Chenhua CHI660 electrochemical workstation. The light source was provided by a quartz optical fiber (working spot diameter: 5 mm) equipped with a xenon lamp with an irradiation intensity of 300 mW/cm^2 (PLS-SXE300, Beijing Perfect Lighting Co., Ltd.). The sample of SAC Cu-TiO_2 and TiO_2 powder (2 mg) were ultrasonically dispersed in 0.2 mL ink, which consisted of water, ethanol and Nafion in a volumetric ratio of 60:35:5. The resultant suspension (20 μL) was dropped onto a glassy carbon electrode, which was further dried at 60 °C for 3 h. The prepared catalyst, saturated calomel electrode (SCE) and a platinum wire (0.1 mm) were used as the working, reference and counter electrodes, respectively. In 10 mL of 0.1 M $KHCO_3$ + 100 ppm KNO_3 solution with saturated CO_2, the in-situ photoelectrochemical infrared spectra were tested with real-time potential. When in-situ FTIR spectra were collected, the scanned potential range was − 0.3 to − 0.8 V with a step size of 0.1 V under light or dark condition.

2.5. Computational method

The Vienna Ab-initio Simulation Package (VASP) [34,35] was employed to perform all density functional theory (DFT) calculations within the generalized gradient approximation (GGA) using the PBE

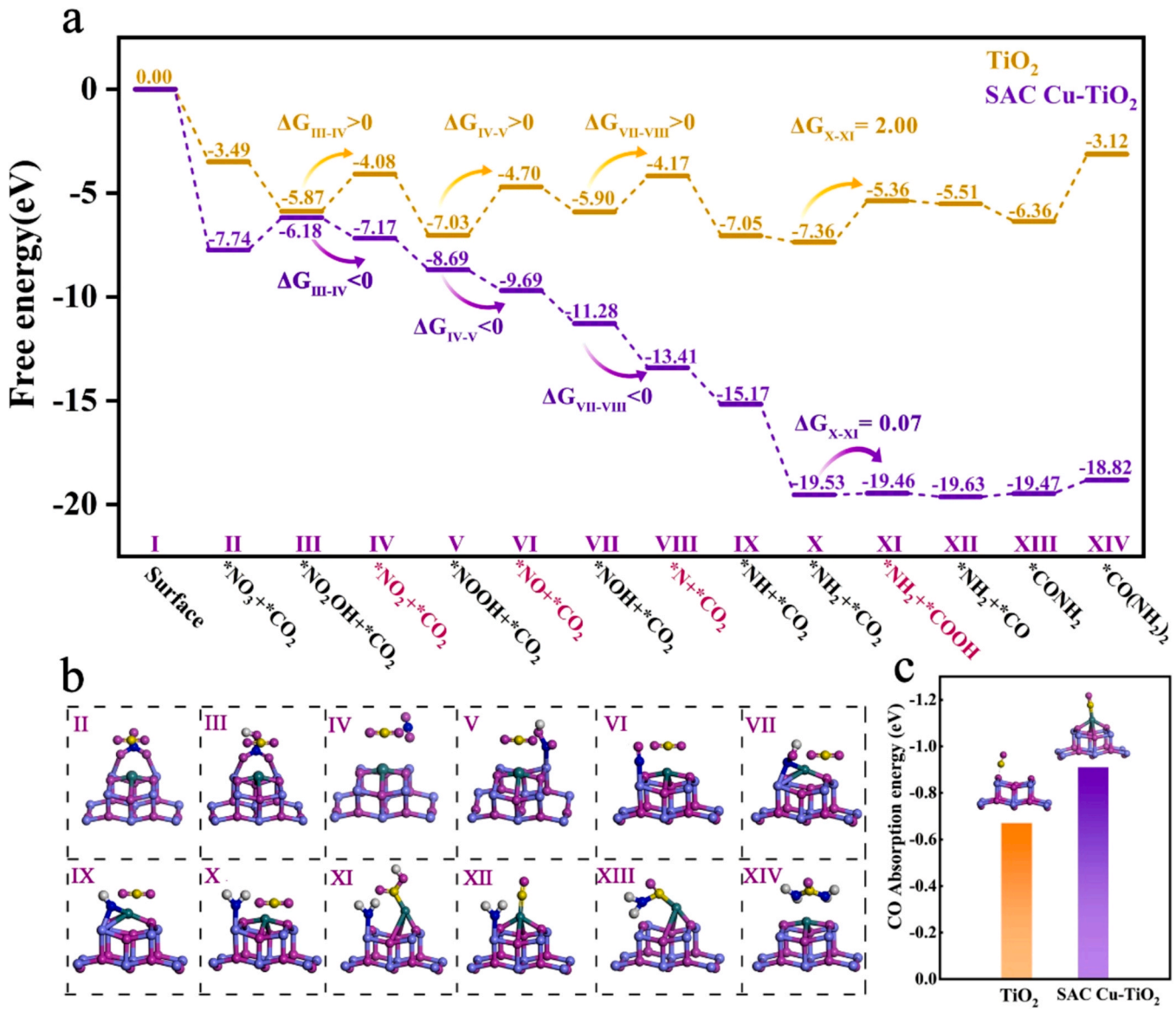

Fig. 1. DFT calculations for pathway of urea synthesis. (a) Free energy of the intermediates on TiO_2, SAC Cu-TiO_2, (b) Optimized intermediate structures in the pathway for urea synthesis on SAC Cu-TiO_2, (c) Absorption energy of CO on TiO_2 and SAC Cu-TiO_2. The green, purple, blue, yellow, wathet blue, and grey balls represent Cu, O, N, C, Ti, and H atoms, respectively.

formulation [36]. We have chosen the projected augmented wave (PAW) potentials [37,38] to describe the ionic cores and take valence electrons into account using a plane wave basis set with a kinetic energy cutoff of 450 eV. Partial occupancies of the Kohn−Sham orbitals were allowed using the Gaussian smearing method and a width of 0.05 eV. The on-site corrections (DFT + U) has been applied to the 3d electron of Ti atoms (Ueff = 4.5 eV) by the approach from Dudarev et al. [39] The electronic energy was considered self-consistent when the energy change was smaller than 10 − 5 eV. A geometry optimization was considered convergent when the force change was smaller than 0.02 eV/Å. Grimme's DFT-D3 methodology [40] was used to describe the dispersion interactions. The equilibrium lattice constants of the anatase TiO_2 unit cell were optimized using a 10 × 10 × 4 Monkhorst-Pack k-point grid for Brillouin zone sampling (a = b = 3.858 Å and c = 9.652 Å). We then used it to construct a TiO_2 (001) surface model (model 1) with p (3 × 2) periodicity in the X and Y directions and one stoichiometric layer in the Z direction by vacuum depth of 15 Å in order to separate the surface slab from its periodic duplicates. The SAC Cu-TiO_2 (model 2) was built by adding one Cu atom onto TiO_2 (001). During structural optimization, a 1 × 2 × 1 in the Brillouin zone was used for k-point sampling, and the bottom half stoichiometric layer was fixed, while the rest were allowed to fully relax.

The adsorption energy (E_{ads}) of adsorbate A was defined as :

$$E_{ads} = E_{A/surf} - E_{surf} - E_{A(g)}$$

where $E_{A/surf}$, E_{surf} and $E_{A(g)}$ are the energy of adsorbate A adsorbed on the polyimide, the energy of clean polyimide, and the energy of isolated A molecule in a cubic periodic box with a side length of 20 Å and a 1 × 1 × 1 Monkhorst-Pack k-point grid for Brillouin zone sampling, respectively.

The transition state of an elementary reaction step was located by the nudged elastic band (NEB) method [41]. In the NEB method, the path between the reactant(s) and product(s) was discretized into a series of five structural images. The intermediate images were relaxed until the perpendicular forces were smaller than 0.02 eV/Å. The free energy of a gas phase molecule or an adsorbate on the surface was calculated by the equation G = E + ZPE − TS, where E is the total energy, ZPE is the zero-point energy, T is the temperature in kelvin (298.15 K is set here),

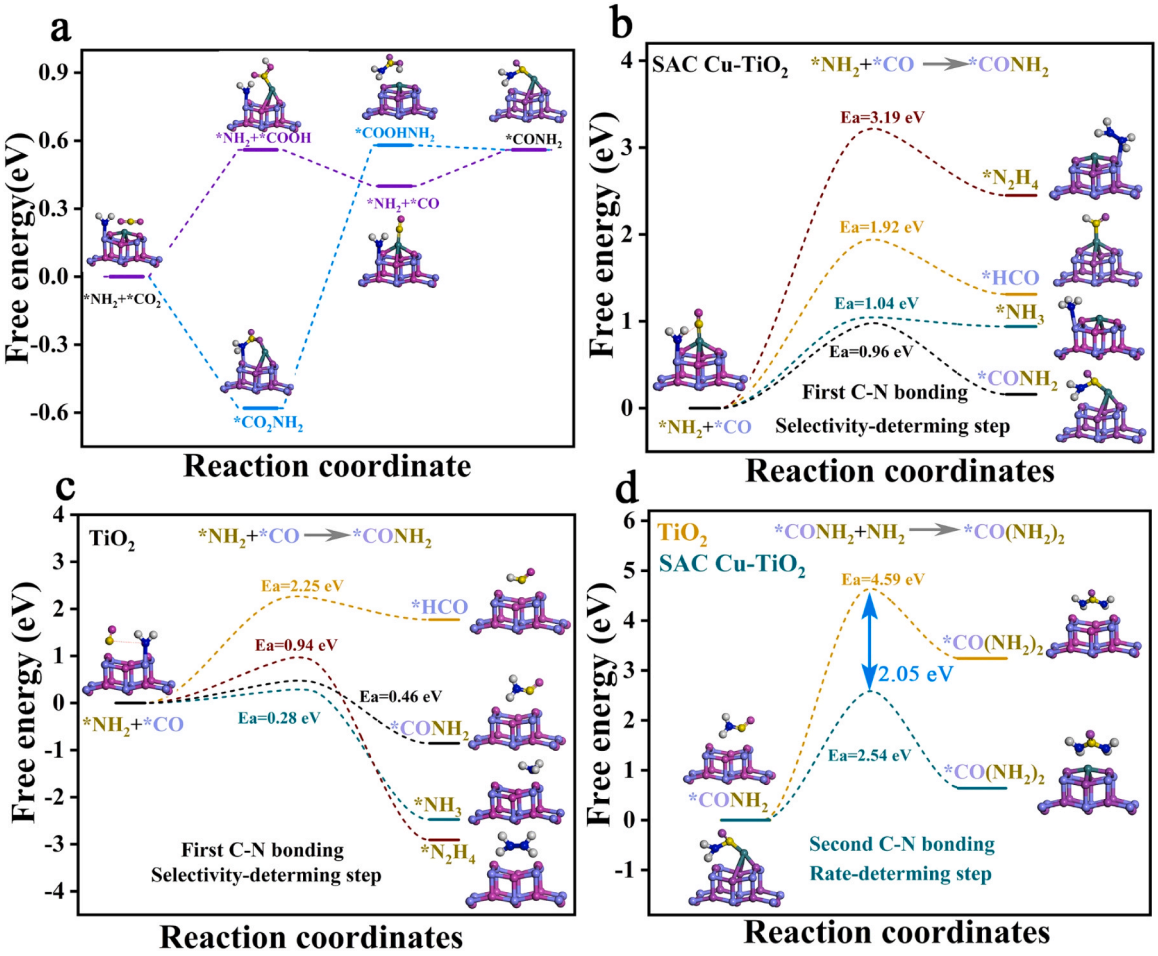

Fig. 2. (a) Free energy of formation $*CONH_2$ from $*NH_2$ and $*CO_2$, diagram of free energy changes and activation barriers of *CO and $*NH_2$ coupled to $CONH_2$ and other parallel CO_2/NO_3- reduction reaction on (b) SAC Cu-TiO_2, (c) TiO_2, (d) $*CO(NH_2)_2$ formation from $CONH_2$ on TiO_2 and SAC Cu-TiO_2.

and S is the entropy. The reported standard hydrogen electrode (SHE) model [40] was adopted in the calculations of Gibbs free energy changes (ΔG) of all reaction steps, which was used to evaluate the reaction barrier. The chemical potential of a proton-electron pair, $\mu(H^+) + \mu(e^-)$, is equal to the half of the chemical potential of one gaseous hydrogen molecule, $1/2\ \mu(H_2)$, at U = 0 V.

3. Results and discussion

3.1. Theoretical predictions of the structure-performance relationship

To provide insight into the active sites and reaction pathway for urea synthesis from nitrate and CO_2, we carried out DFT calculations to investigate the energy barrier for production of urea on SAC Cu-TiO_2 and TiO_2 (Fig. 1**a**). The reaction mechanism of urea synthesis is that the nitrate reduction intermediates $*NH_2$ and CO_2 reduction intermediates *CO are coupled via C-N bonding, in which the formation of $*NH_2$ and *CO intermediates is the key step. In the process of reduction of nitrate to the $*NH_2$ intermediate, the energy barriers of $*NO_2OH$ reduction to $*NO_2$, *NOOH reduction to *NO, and the hydrogenation of *NOH to *N are all greater than 0, which means that these processes are not spontaneous over pure TiO_2. However, these critical steps are an exothermic reaction (ΔG<0) on the SAC Cu-TiO_2, which occurs spontaneously and easily on Ti site of SAC Cu-TiO_2. From the free energy change diagram, single atom copper anchored on TiO_2 is easier to reduce nitrate to $*NH_2$ intermediates than pure TiO_2, which may be attributed to that Cu single atom introduced TiO_2 change the electronic structure of Ti 3d orbital of TiO_2, that the Ti 3d states crossed the Fermi level only in SAC Cu-TiO_2 (Fig. S1), indicating that the Ti sites had higher activity for nitrate reduction to $*NH_2$ in SAC Cu-TiO_2 than TiO_2. In the process of CO_2 reduction to the *CO intermediate, CO_2 hydrogenation to *COOH is the critical step. The energy barrier of $*CO_2$ reduction to *COOH is only 0.07 eV on Cu site of SAC Cu-TiO_2, but that of $*CO_2$ hydrogenation to *COOH is 2 eV over TiO_2. This means that hydrogenation of CO_2 to *COOH intermediates is more likely to occur on SAC Cu-TiO_2. It is worth noting that when the *COOH is reduced to *CO intermediate, the strong interaction between CO intermediate and single atom Cu site in SAC Cu-TiO_2 is observed by the partial density of states (PDOS) (Fig. S2c). In contrast, the interaction between *CO intermediate and Ti site in TiO_2 and CuO are relatively weak (Fig. S2a, **b**). The *CO intermediate is adsorbed on single atom Cu with bond length (Cu-C atom) 1.797 Å. Compared with bond length of *CO intermediate adsorbed on TiO_2 (2.349 Å), it has strong adsorption energy to *CO intermediates with −0.91 eV by Cu single atom, making it not easy to desorb to form by-product CO (Fig. 1**c**). This is conducive to its subsequent coupling reaction with $*NH_2$. In a word, compared with TiO_2, the anchoring of single atom Cu on TiO_2 engineered unique dual metal Cu and Ti active sites is beneficial for the reduction of nitrate to $*NH_2$ and reduction of CO_2 to *CO. Finally, from the free energy change of reduction nitrate and CO_2 to synthesize urea, it can be seen that SAC Cu-TiO_2 has a lower free energy to urea synthesis. The process of C-N coupling of nitrate and CO_2 for urea synthesis at Ti and Cu sites of SAC Cu-TiO_2 was investigated DFT calculations (Fig. 1**b**). The two oxygen atoms of nitrate are bridged onto the Ti site, while CO_2 is adsorbed onto the single atom Cu site, which is consistent with the results detected by in-situ FT-IR spectroscopy (Fig. 5**b**). Nitrate is reduced to $*NO_2OH$ at the Ti site of SAC Cu-

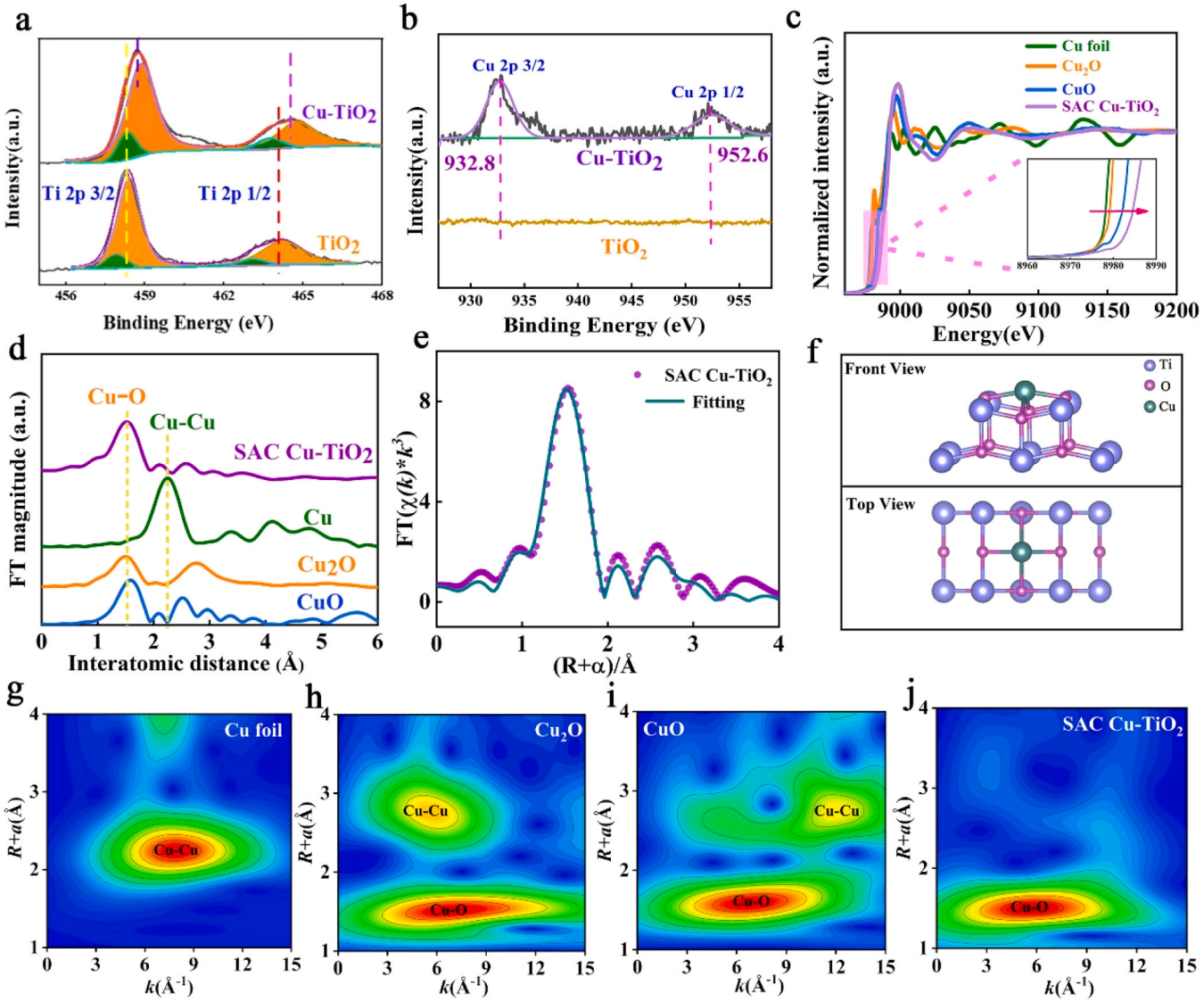

Fig. 3. (a) Ti 2p XPS spectra, (b) Cu 2p XPS spectra, (c) XANES of Cu foil, Cu_2O, CuO and SAC Cu-TiO_2, (d) FT-EXAFS spectra at Cu foil, and Cu_2O, CuO and SAC Cu-TiO_2, (e) Fourier transform of the Cu K-edge of the EXAFS spectra of SAC Cu-TiO_2 and R space fitting curves, (f) coordination structure of SAC Cu-TiO_2, Wavelet transform for k3-weighted EXAFS spectra of (g) Cu foil, (h) Cu_2O, (i) CuO and (j) SAC Cu-TiO_2.

TiO_2, which is then hydrogenated to form the $*NO_2$ intermediate. The intermediate NO_2 undergoes further hydrogenation to generate NOOH on Ti site of SAC Cu-TiO_2. After multiple hydrogenation processes, $*NH_2$ intermediate is formed on Ti site of SAC Cu-TiO_2 ($*NO_3^- \rightarrow *NO_2OH \rightarrow *NO_2 \rightarrow *NOOH \rightarrow *NO \rightarrow *NOH \rightarrow *N \rightarrow *NH \rightarrow *NH_2$). On the other hand, the CO_2 adsorbed on single atom Cu site is reduced to form *COOH, which is reduced to *CO intermediate on Cu site ($*CO_2 \rightarrow$ *COOH $\rightarrow$*CO). It is also consistent with the results detected by in-situ FT-IR spectroscopy (Fig. 5**e**). The *CO intermediate adsorbed on the single atom Cu site is coupled with $*NH_2$ on the adjacent Ti site to generate $*CONH_2$. Then, $*CONH_2$ intermediate continues to couple with the $*NH_2$ intermediate adsorbed on the Ti site to generate urea ($*CO + *NH_2 \rightarrow *CONH_2 \rightarrow *CO(NH_2)_2$).

The reaction mechanisms of two-step C-N bonding of CO_2 and nitrate reduction intermediates to synthesize urea are discussed in detail by DFT calculations. In the first step of C-N bonding generated $*CONH_2$ intermediate for urea synthesis, the adsorbed CO_2 and nitrate reduction intermediate may be coupled in advance. It is speculated that $*CO_2$ and $*NH_2$ are directly coupled to generate $*CO_2NH_2$, which undergoes a two-step hydrogenation process to generate $*CONH_2$ intermediate (Fig. 2**a**) ($*CO_2 + *NH_2 \rightarrow *CO_2NH_2 \rightarrow *COOHNH_2 \rightarrow *CONH_2$). Another pathway of the first C-N coupling to generate $*CONH_2$ is also discussed that CO_2 is reduced to *CO intermediate, and the NO_3^- is reduced to $*NH_2$ intermediate, and then C-N coupling is performed to generate $*CONH_2$. ($*NH_2 + *CO_2 \rightarrow *NH_2 + *COOH \rightarrow *CO + *NH_2 \rightarrow *CONH_2$).

Comparing the two reaction paths for urea generation by theoretical calculations, the highest free energy of the *CO and $*NH_2$ coupling pathway ($*NH_2 + *COOH \rightarrow 0.56$ eV) is lower than that of $*CO_2$ and $*NH_2$ coupling ($*COOHNH_2 \rightarrow 0.59$ eV). Therefore, the *CO and $*NH_2$ coupling path is more likely to generate urea. However, during *CO and $*NH_2$ coupling to generate $*CONH_2$, parallel competitive reactions of NO_3^- and CO_2 may occur, the most important of which is the hydrogenation and dimerization of the intermediates $*NH_2$ and *CO, which seriously affect the efficiency of C-N bonding by $*NH_2$ and *CO coupling. The first C-N bonding of *CO and $*NH_2$ is the selectivity-determining step for urea synthesis ($*CO + *NH_2 \rightarrow *CONH_2$). From the changes of the free energy of the parallel competing reactions of $*NH_2$ and *CO, it is found that NH_3 and N_2H_4 are more easily generated by hydrogenation and dimerization of $*NH_2$ intermediates on TiO_2 (Fig. 2**c**). The coupling of *CO and $*NH_2$ to generate $*CONH_2$ intermediate at distant Ti and Ti sites (3.9 Å) on TiO_2 does not easily occur due to the weak nucleophilic attack of $*NH_2$ to *CO intermediate with a long distance between them.

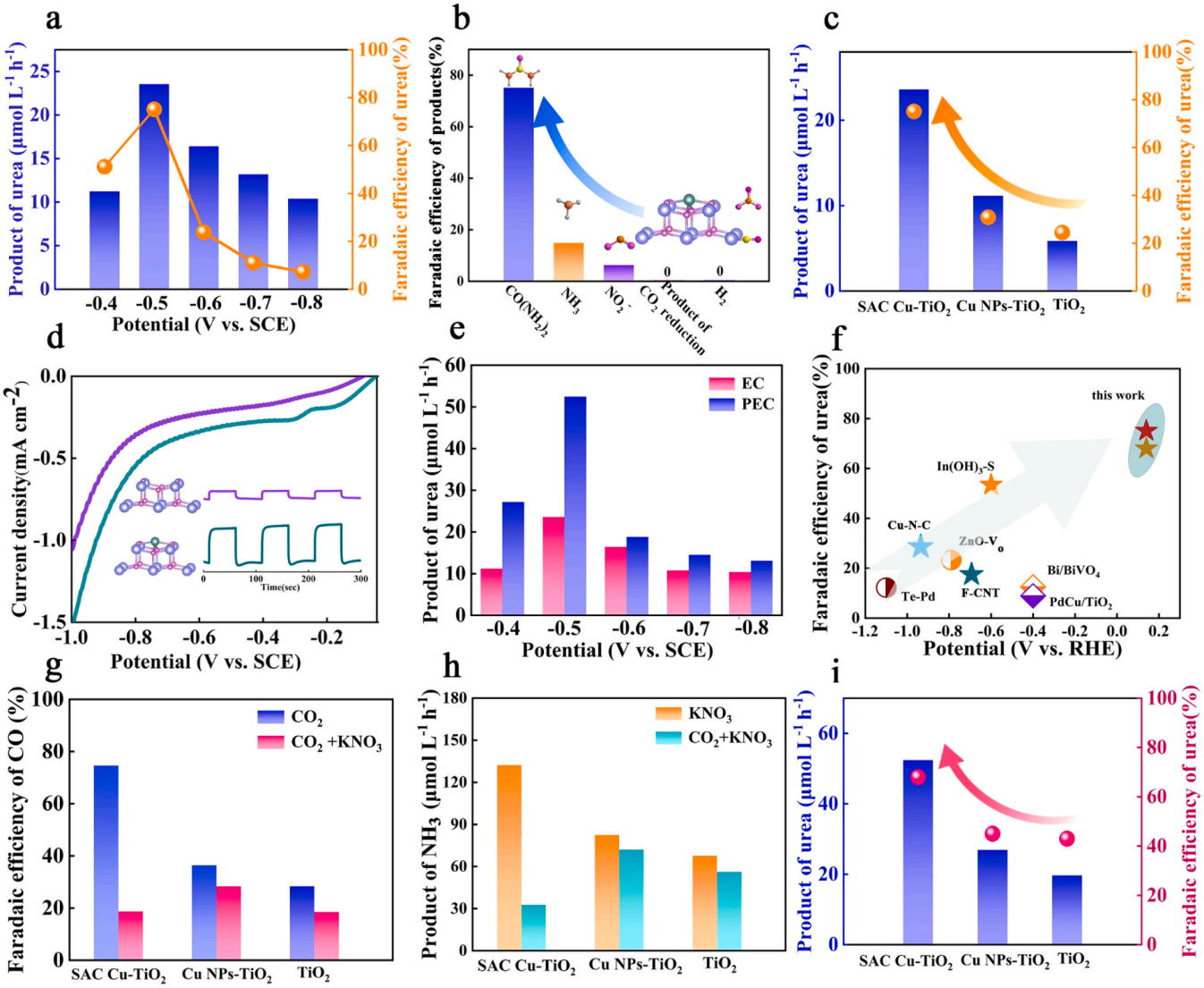

Fig. 4. (a) yield and Faradaic efficiency of urea on SAC Cu-TiO_2 at different voltages, (b) the Faradaic efficiency of various products, (c) yield and Faradaic efficiency of urea on SAC Cu-TiO_2 and TiO_2 at − 0.5 V, (d) LSV curves and i-t of SAC Cu-TiO_2 and TiO_2 in CO_2 and NO_3^-, (e) yield of urea by PEC and EC at different voltages, (f) literatures of recorded results for urea synthesis, (g) Faradaic efficiency of CO on SAC Cu-TiO_2, Cu NPs-TiO_2 and TiO_2 in 0.1 M $KHCO_3$ solution of CO_2 atmosphere with or without 100 ppm KNO_3, (h) the yield of NH_3 on SAC Cu-TiO_2, Cu NPs-TiO_2 and TiO_2 in 0.1 M $KHCO_3$ + 100 ppm KNO_3 solution with or without CO_2, (i) the yield and Faradaic efficiency of urea on SAC Cu-TiO_2, Cu NPs-TiO_2 and TiO_2 in 100 ppm KNO_3 + 0.1 M $KHCO_3$ solution of CO_2 atmosphere at − 0.5 V and light.

However, the reaction pathway is changed by constructing dual metal Cu and Ti active sites with short distance of 2 Å by anchoring Cu atoms onto TiO_2. The distance between Cu and Ti sites on SAC Cu-TiO_2 is about half that of Ti and Ti sites on TiO_2. Therefore, compared to the free energies for the formation of HCO, NH_3 and N_2H_4, the selective coupling of *CO and $*NH_2$ to generate $*CONH_2$ intermediate at the close Cu and Ti sites with short distance (2 Å) on SAC Cu-TiO_2 has the lowest free energy (Fig. 2**b**). It was confirmed that C-N bonding occurs more easily than parallel competing reactions of NO_3^- and CO_2 on SAC Cu-TiO_2, which is an important reason for the efficient synthesis of urea. The formation of urea from nitrate and CO_2 requires two steps of C-N bonding, in which the first C-N bonding is a selectivity-determining step ($*CO+NH_2 \rightarrow *CONH_2$), while the second C-N bonding is a rate-determining step. By comparing the activation energy of the coupling of $*CONH_2$ and $*NH_2$ to form urea, it can be seen that compared with pure TiO_2 (distance between Ti and Ti sites of 3.9 Å), constructing dual metal Cu and Ti active sites by single atom Cu supported on TiO_2 reduces the reaction energy barrier of $*CONH_2$ and $*NH_2$ coupling on Cu and Ti active sites with short distance (2 Å) for its directional coupling between nearby reaction intermediates. The activation energy of $*CONH_2 + NH_2 \rightarrow *CO(NH_2)_2$ decreased from 4.59 eV to 2.54 eV after anchoring Cu atoms onto TiO_2, which makes the second step C-N bonding more likely to occur and easier to generate urea (Fig. 2**d**).

3.2. *Structural characterization of single atom photoelectrocatalyst*

Inspired by the theoretical results, we prepared and characterized SAC Cu-TiO_2 and TiO_2. The prepared TiO_2 exhibits a nanosheet-like structure characterized by scanning electron microscopy and transmission electron microscopy (Fig. S3a). The atomic dispersion Cu species anchored on TiO_2 nanosheets is achieved by a previously reported precipitation method [33]. After anchoring Cu species, the microstructure of TiO_2 remained unchanged. The prepared TiO_2 and SAC Cu-TiO_2 with nanosheet-like structures were well crystallized anatase and the main diffraction peaks in the pattern are identical with the standard card (JCPDS PDF #21–1272) (Fig. S3b). Due to the low content or high dispersion of Cu species, characteristic diffraction peaks of Cu species aren't observed in the X-ray diffraction (XRD) pattern in Cu-TiO_2. To

further explore whether Cu species were deposited on TiO_2, the elemental distribution was measured by EDS (Fig. S3c). The Ti, O and Cu elements were uniformly distributed, indicating that Cu species had been deposited onto TiO_2 nanosheets. The elemental composition and chemical state of the catalysts were further investigated by X-ray photoelectron spectroscopy (XPS) (Fig. 3**a**). The binding energy (BE) of Ti 2p3/2 and 2p1/2 in TiO_2 were located at 458.3 eV and 464 eV, indicating that Ti of TiO_2 existed in the chemical valence state of + 4 [42]. The BE of Ti in Cu-TiO_2 is shifted slightly to 458.7 eV and 464.5 eV. The shift of the BE is ascribed to the electronic interactions and charge transfer between Ti and Cu species. In the Cu 2p XPS spectra of Cu-TiO_2 and TiO_2, no Cu 2p peak was observed in TiO_2. And the binding energy of Cu 2p3/2 and 2p1/2 in Cu/TiO_2 located at 932.8 and 952.6 eV (Fig. 3**b**), which indicates that the copper species were also successfully anchored to the TiO_2 and the Cu species is present in the chemical state of + 1. The reduction of Cu^{2+} species to Cu^{+} can be achieved by the bombardment effect of X-ray irradiation during XPS analysis under high vacuum and in the presence of a very low copper content with a highly dispersed state [33]. Therefore, the valence state of copper in Cu-TiO_2 was further analyzed by Cu K-edge X-ray absorption near-edge structure (EXANES) spectroscopy (Fig. 3**c**). The XANES spectrum of the Cu K-edge of Cu-TiO_2 shows that the absorption edge was behind that of CuO, indicating that the valence of Cu in Cu-TiO_2 is about + 2. It can be seen that the chemical environment of Cu^{2+} species in Cu-TiO_2 was similar to that of Cu^{2+} species in CuO, but the Cu species in Cu-TiO_2 had strong scattering only in the first shell and no scattering existed in other shells, which indicates that the prepared copper species is single atom. This conclusion was further proved by wavelet transform. By comparing the wavelet transforms of Cu foil Cu_2O, CuO and SAC Cu-TiO_2 (Fig. 3**g-j**), It can be seen there are only Cu-O bonds but no Cu-Cu bonds in SAC Cu-TiO_2, which also shows that Cu species existed as a form of single atom. The coordination number of copper single atom was explored by EXAFS fitting of the SAC Cu-TiO_2 at the Cu K-edge (Fig. 3**e**). The fitting analysis showed that the Cu atom was connected to four O atoms in the first coordination shell, which means that the Cu atom was attached to the surface of TiO_2 by four coordinates with oxygen atoms. The structure diagram of SAC Cu-TiO_2 is shown in Fig. 3**f**.

3.3. Photoelectrocatalytic synthesis of urea performance evaluation

Compared with TiO_2, the SAC Cu-TiO_2 showed better photoelectrocatalytic performance for the synthesis of urea from CO_2 and nitrate. Firstly, compared with TiO_2, SAC Cu-TiO_2 had stronger light absorption in the range of 500–800 nm (Fig. S4a). And SAC Cu-TiO_2 had a larger photoresponse current reaching 4 μA/cm^2, which is five times greater than that of TiO_2 (0.8 μA/cm^2) (Fig. 4**d**). This indicates that Cu species promoted the separation of photogenerated electrons and holes. Secondly, the impedances of SAC Cu-TiO_2 and TiO_2 catalysts were compared, and the smaller electrochemical impedance of SAC Cu-TiO_2 was favorable for electron transfer (Fig. S4c). Finally, through the linear scan curve test in 0.1 M $KHCO_3$ solution containing 100 ppm KNO_3 with saturated CO_2 atmosphere (Fig. 4**d**), it can be seen that the photoelectrocatalytic current of SAC Cu-TiO_2 was higher than that of TiO_2, indicating that SAC Cu-TiO_2 was conducive to urea synthesis from nitrate and CO_2. Evaluation of performance of photoelectrocatalytic synthesis of urea on SAC Cu-TiO_2 was tested in an H-cell reactor at fixed potentials and under light irradiation (Fig. S5). The concentration of urea was measured by the diacetyl monoxime method (Fig. S6). Firstly, the yield of urea was evaluated over SAC Cu-TiO_2 at different voltages (Fig. 4**a**). The yield of urea is the highest at − 0.5 V, reaching 23.6 μmol L^{-1} h^{-1}, corresponding to faradaic efficiency of 75.1%, which is 3.07 times higher than that of TiO_2, respectively (Fig. 4**c**). And it is the highest Faradaic efficiency of synthetic urea ever reported (Fig. 4**f**). The reason is that the absence of CO_2 parallel reduction reactions and hydrogen evolution side reactions are important factors for its efficient urea synthesis by electrocatalysis (Fig. 4**b**). The detailed reaction mechanism of electrocatalytic synthesis of urea is also clearly discussed in DFT calculations section (Fig. 2**a**). The tests of photoelectrochemical synthesis of urea were carried out under different voltages (range of −0.4 V to −0.8 V) and light over SAC Cu-TiO_2 (Fig. S11). The SAC Cu-TiO_2 has the better photoelectrocatalysis performance to C-N bonding for synthesis urea under the conditions of light and voltage − 0.5 V (PEC) than pure − 0.5 V (EC), the yield of urea reached 53.45 μmol L^{-1} h^{-1} (Fig. 4**e**), which was 2.2 times higher than that of pure electrocatalysis. To ensure the accuracy of the data, we also used ^{1}H NMR method to detect the yield of urea produced by photoelectrocatalytic reduction of nitrate and CO_2 over SAC Cu-TiO_2 under the conditions of light and voltage − 0.5 V after 1 h. Based on the calibration curves about peak area of ^{1}H NMR and concentration of urea (Fig. S12a**, b**), the concentration of urea after photoelectrocatalytic reduction reaction detected by ^{1}H NMR method was consistent with the concentration detected by UV-Vis through diacetyl monoxime method (Fig. S12c). For the long-term stability test, the test of photoelectrochemical synthesis of urea was carried out for 10 h. There is no significant decrease in current density, which indicated that SAC Cu-TiO_2 is relatively stable (Fig. S13). The reason why SAC Cu-TiO_2 can efficiently promote C-N coupling by photoelectrocatalysis for urea synthesis from CO_2 and nitrate were revealed by comparing the reduction products in independent system and a coexisting system of CO_2 and nitrate. When one of the reactants of CO_2 and nitrate is not present, urea cannot be synthesized over SAC Cu-TiO_2 (Fig. S14), indicating that the CO_2 and nitrate are the C and N sources for urea synthesis. In the independent system (Fig. 4**g, h**), it is shown that the single atom Cu anchored on TiO_2 is favorable for reduction of CO_2 to CO and nitrate to ammonia. When only the CO_2 reduction reaction occurred in $KHCO_3$ solution under a saturated CO_2 atmosphere on SAC Cu-TiO_2, the Faradaic efficiency of CO_2 reduction to CO was 74.6%, which was 2.64 time that of TiO_2. However, when C-N coupling occurred during urea synthesis in 0.1 M $KHCO_3$ + 100 ppm KNO_3 solution with CO_2, the Faradaic efficiency of the by-product CO was only 18.7% over SAC Cu-TiO_2 (Fig. 4**g**). This shows that SAC Cu-TiO_2 can promote the reduction of CO_2 to *CO intermediates, and at the same time, it can promote efficient C-N bond with the reduction intermediates of nitrates. In another hand, the nitrate can be also efficiently reduced to ammonia on SAC Cu-TiO_2 in 0.1 M $KHCO_3$ + 100 ppm KNO_3 solution without CO_2. The ammonia yield was 132.18 μmol L^{-1} h^{-1}, which was 4.04 times that of TiO_2. In 0.1 M $KHCO_3$ + 100 ppm KNO_3 solution with CO_2, the C-N coupling for synthesis urea can occur, and the yield of ammonia dropped sharply achieving 32.7 μmol L^{-1} h^{-1} on SAC Cu-TiO_2 (Fig. 4**h**). From the yield results of CO_2 and nitrate coupling to generate urea, it can also be seen that SAC Cu-TiO_2 is conducive to the simultaneous reduction of nitrate and CO_2 to promote C-N coupling to generate urea. Finally, this conclusion is also proved by the yield of urea over SAC Cu-TiO_2 and TiO_2 (Fig. 4**i**). The yield and FE of urea on SAC Cu-TiO_2 was 52.45 μmol L^{-1} h^{-1} and 68%, while the yield of urea on TiO_2 was only 19.67μmol L^{-1} h^{-1} under the conditions of light and voltage of − 0.5 V. In addition, the effect of various loading of Cu single atoms on urea synthesis was explored. The Cu content of the SAC Cu TiO_2 catalyst we prepared was analyzed by ICP-MS, it was found that the Cu content was 0.58 wt%. As the content of Cu loaded onto TiO_2 increases, the copper species may undergo aggregation, which weakened the catalytic performance of urea synthesis (Fig. S15).

3.4. In-situ characterization of the catalytic mechanism for urea synthesis

To gain insight into the process of urea synthesis from nitrate and CO_2, the reaction intermediates were detected by in-situ infrared spectroscopy. In-situ infrared spectroscopy and DFT calculations mutually confirm the reaction pathway of urea synthesis from CO_2 and nitrate over the catalyst. Firstly, the adsorption of CO_2 and nitrate on the catalyst was detected by infrared spectroscopy. The TiO_2 can effectively adsorb nitrate. The absorption peaks of nitrate were observed at 1055,1240 and 1620 cm^{-1}, indicating that it is a bridge adsorbed nitrate

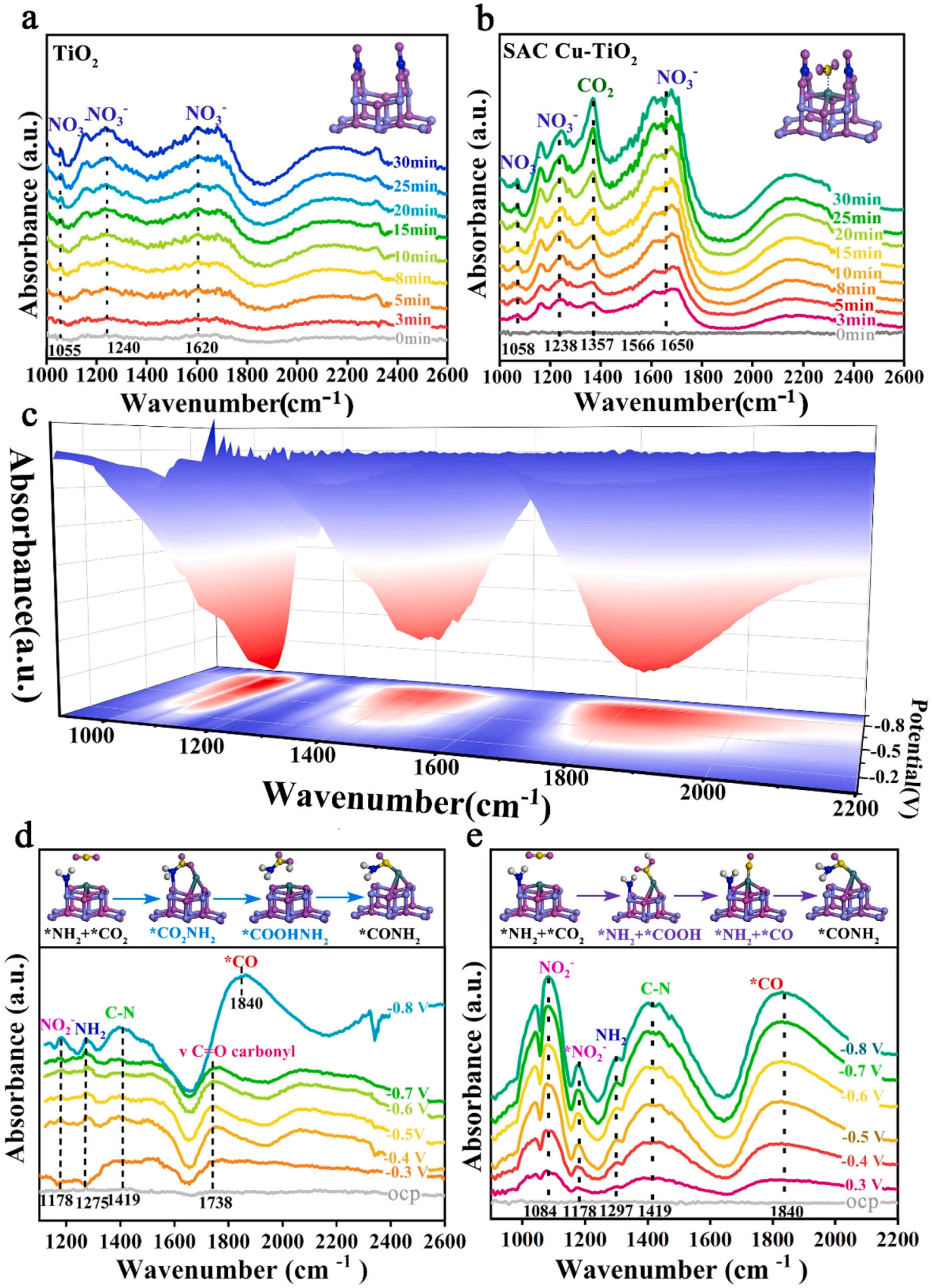

Fig. 5. FT-IR detection of adsorbed CO_2 and nitrate on (a) TiO_2 and (b) SAC Cu-TiO_2, (c) three-dimensional in-situ FT-IR spectra photoelectrocatalysis (PEC) of CO_2 and nitrate for synthesis urea on SAC Cu-TiO_2, in-situ FT-IR detection of catalytic intermediates in electrocatalysis (EC) (d) and photoelectrocatalysis (PEC) (e) of CO_2 and nitrate for synthesis urea on SAC Cu-TiO_2.

on TiO_2 [43]. But the absorption peak of CO_2 wasn't detected, indicating that TiO_2 has weak ability to adsorb CO_2 (Fig. 5**a**). However, single atom Cu anchored on TiO_2 is favourable for simultaneous adsorption of nitrate and CO_2. Besides the absorption peaks of nitrate, a new absorption peak of 1640 cm^{-1} was observed on SAC Cu-TiO_2, which was a CO_2 absorption peak and indicating monodentate adsorption on single atom copper (Fig. 5**b**) [44]. This may be attributed to the strong hybridization overlap between the Cu 3d orbital of Cu atom and C 2p orbital of CO_2. In the process of the synthesis of urea from nitrate and CO_2, the wavelength changes of reaction intermediates were detected by in-situ infrared spectroscopy. During the electrocatalytic urea synthesis from nitrate and CO_2, $*NH_2$ intermediate, carbonamide intermediate and C-N bonding were observed corresponding peaks at 1275 cm^{-1}, 1738 cm^{-1} and 1419 cm^{-1}, respectively (Fig. 5**d**) [8,45,46]. Therefore, it is speculated that the mechanism of electrocatalytic generation of urea from CO_2 and nitrate is that $*NH_2$ and adsorbed $*CO_2$ are coupled, and the intermediate $*H_2NCOOH$ is generated after one-step hydrogenation, which generates urea through a multi-step process. It corresponds to the reaction path ($*CO_2 + *NH_2 \rightarrow *CO_2NH_2 \rightarrow *COOHNH_2 \rightarrow *CONH_2$) in the theoretical calculation section. However, during the photoelectrocatalytic synthesis of urea from nitrate and CO_2, the obvious absorption peaks of ammonia intermediate (1297 cm^{-1}) and *CO intermediate (1840 cm^{-1}) were detected (Fig. 5**c, e**) [45,47]. At the same time, there was a strong absorption peak at 1419 cm^{-1} corresponding to C-N bonding [8]. Therefore, the pathway of photoelectrocatalytic synthesis of urea is that $*NH_2$ and *CO intermediates were coupled with C-N bonding to form $*CONH_2$, which corresponds to the reaction path ($*CO_2 + *NH_2 \rightarrow *COOH + *NH_2 \rightarrow *CO + *NH_2 \rightarrow *CONH_2$) in the theoretical calculation section. In addition, the mechanism of C-N coupling for photoelectrocatalysis reduction of CO_2 and isotope-labelling nitrate ($^{15}NO_3^-$) was investigated through FT-IR spectroscopy over SAC Cu-TiO_2. Compared with the measurements without isotope-labelling (Fig. 5**e**), the vibrations of $^{15}NO_2^-$, $^{15}NH_2$ and C-^{15}N with isotope-labelling of N are moved towards lower wavenumbers by 10 – 20 cm^{-1} (Fig. S16). It is attributed to isotope effect [48]. The reaction intermediates detected by in-situ infrared spectroscopy further verified the theoretical calculations of the reaction pathway.

4. Conclusion

In this work, we efficiently promoted efficient urea synthesis and suppressed side reactions in the process of photoelectrocatalytic reduction of nitrate and CO_2 via close Cu/Ti bimetallic sites by anchoring single atom Cu onto TiO_2. The SAC Cu-TiO_2 had faster reaction kinetics with a Faradic efficiency of 68% for urea synthesis under the condition of light irradiation and − 0.5 V. The nitrate reduction intermediate $*NH_2$ and CO_2 reduction intermediate *CO selectively coupled at the close Cu and Ti sites on SAC Cu-TiO_2 for urea synthesis. The SAC Cu-TiO_2 is beneficial to adsorb its reaction intermediate *CO, making it difficult to desorb and inhibiting the side reaction of CO_2 reduction to CO, which is conducive to its subsequent coupling reaction with $*NH_2$. And compared with their parallel competing CO_2/NO_3^- reduction reactions such as *CO hydrogenation, $*NH_2$ hydrogenation and its dimerization, the coupling of *CO and $*NH_2$ formation C-N bonding had a lower energy barrier by anchoring single atom Cu onto TiO_2. This is an important reason for the efficient synthesis of urea over SAC Cu-TiO_2. We deduced the reaction mechanism of C-N coupling through experimental results of CO_2 and nitrate reduction products and in-situ infrared spectroscopy detecting the adsorption and catalytic reaction intermediates in the process of reduction of NO_3^- and CO_2 to urea.

CRediT authorship contribution statement

Jingui Zheng: Formal analysis, Data curation, Writing – original draft. **Shaohan Xu**: Investigation, Supervision. **Jie Sun**: Writing – review & editing, Data curation. **Jinxing Zhang**: Validation, Supervision. **Lingzhi Sun**: Data curation, Formal analysis. **Pan Xun**: Visualization, Formal analysis. **Lina Li**: Software, Methodology. **Guohua Zhao**: Conceptualization, Project administration, Supervision, Funding acquisition.

Declaration of Competing Interest

The authors declare no conflict of interest.

Data availability

Data will be made available on request.

Acknowledgements

This research was financially supported by the Natural Science Foundation of China (NSFC, Nos. 21876128, 22076140 and 21537003). Additionally, we acknowledge the help from Shanghai Synchrotron Radiation Facility (SSRF, Nos. 2022-SSRF-PT-020439, 2022-SSRF-PT-020432).

Appendix A. Supporting information

Supplementary data associated with this article can be found in the online version at doi:10.1016/j.apcatb.2023.123056.

References

[1] Y. Ou, C. Roney, J. Alsalam, K. Calvin, J. Creason, J. Edmonds, A.A. Fawcett, P. Kyle, K. Narayan, P. O'Rourke, P. Patel, S. Ragnauth, S.J. Smith, H. McJeon, Deep mitigation of CO_2 and non-CO_2 greenhouse gases toward 1.5 °C and 2 °C futures, Nature Commun. 12 (2021) 6245.
[2] S.K. Kim, J. Shin, S. An, H. Kim, N. Im, S. Xie, J. Kug, S. Yeh, Widespread irreversible changes in surface temperature and precipitation in response to CO_2 forcing, Nat. Clim. Change 12 (2022) 834–840.
[3] C. Soued, J.A. Harrison, S. Mercier-Blais, Y.T. Prairie, Reservoir CO_2 and CH_4 emissions and their climate impact over the period 1900–2060, Nat. Geosci. 15 (2022) 700–705.
[4] J. Sun, H. Yang, W. Gao, T. Cao, G. Zhao, Diatomic Pd−Cu Metal-Phosphorus Sites for Complete N—N Bond Formation in Photoelectrochemical Nitrate Reduction, Angewandte Chemie International Edition, 61 (2022) e202211373.
[5] C. Hepburn, E. Adlen, J. Beddington, E.A. Carter, S. Fuss, N. Mac Dowell, J.C. Minx, P. Smith, C.K. Williams, The technological and economic prospects for CO_2 utilization and removal, Nature 575 (2019) 87–97.
[6] N. von der Assen, J. Jung, A. Bardow, Life-cycle assessment of carbon dioxide capture and utilization: avoiding the pitfalls, Energy Environ. Sci. 6 (2013) 2721–2734.
[7] R.G. Grim, Z. Huang, M.T. Guarnieri, J.R. Ferrell, L. Tao, J.A. Schaidle, Transforming the carbon economy: challenges and opportunities in the convergence of low-cost electricity and reductive CO_2 utilization, Energy Environ. Sci. 13 (2020) 472–494.
[8] C. Lv, L. Zhong, H. Liu, Z. Fang, C. Yan, M. Chen, Y. Kong, C. Lee, D. Liu, S. Li, J. Liu, L. Song, G. Chen, Q. Yan, G. Yu, Selective electrocatalytic synthesis of urea with nitrate and carbon dioxide, Nature, Sustainability 4 (2021) 868–876.
[9] C. Lv, C. Lee, L. Zhong, H. Liu, J. Liu, L. Yang, C. Yan, W. Yu, H.H. Hng, Z. Qi, L. Song, S. Li, K.P. Loh, Q. Yan, G. Yu, A defect engineered electrocatalyst that promotes high-efficiency urea synthesis under ambient conditions, ACS Nano 16 (2022) 8213–8222.
[10] X. Liu, P.V. Kumar, Q. Chen, L. Zhao, F. Ye, X. Ma, D. Liu, X. Chen, L. Dai, C. Hu, Carbon nanotubes with fluorine-rich surface as metal-free electrocatalyst for effective synthesis of urea from nitrate and CO_2, Appl. Catal. B: Environ. 316 (2022), 121618.
[11] N. Meng, Y. Huang, Y. Liu, Y. Yu, B. Zhang, Electrosynthesis of urea from nitrite and CO_2 over oxygen vacancy-rich ZnO porous nanosheets, Cell Reports Physical, Science 2 (2021), 100378.
[12] X. Wei, X. Wen, Y. Liu, C. Chen, C. Xie, D. Wang, M. Qiu, N. He, P. Zhou, W. Chen, J. Cheng, H. Lin, J. Jia, X. Fu, S. Wang, Oxygen vacancy-mediated selective C–N coupling toward electrocatalytic urea synthesis, J. Am. Chem. Soc. 144 (2022) 11530–11535.
[13] J. Leverett, T. Tran-Phu, J.A. Yuwono, P. Kumar, C. Kim, Q. Zhai, C. Han, J. Qu, J. Cairney, A.N. Simonov, R.K. Hocking, L. Dai, R. Daiyan, R. Amal, Tuning the coordination structure of Cu-N-C single atom catalysts for simultaneous electrochemical reduction of CO_2 and NO_3^- to urea, advanced energy, Materials 12 (2022) 2201500.
[14] Y. Feng, H. Yang, Y. Zhang, X. Huang, L. Li, T. Cheng, Q. Shao, Te-doped Pd nanocrystal for electrochemical urea production by efficiently coupling carbon dioxide reduction with nitrite reduction, Nano Lett. 20 (2020) 8282–8289.

[15] X. Zhang, X. Zhu, S. Bo, C. Chen, M. Qiu, X. Wei, N. He, C. Xie, W. Chen, J. Zheng, P. Chen, S.P. Jiang, Y. Li, Q. Liu, S. Wang, Identifying and tailoring C-N coupling site for efficient urea synthesis over diatomic Fe-Ni catalyst, Nat. Commun. 13 (2022) 5337.
[16] J. Zhu, M. Xiao, D. Ren, R. Gao, X. Liu, Z. Zhang, D. Luo, W. Xing, D. Su, A. Yu, Z. Chen, Quasi-covalently coupled Ni–Cu atomic pair for synergistic electroreduction of CO_2, J. Am. Chem. Soc. 144 (2022) 9661–9671.
[17] Q. Wang, K. Liu, J. Fu, C. Cai, H. Li, Y. Long, S. Chen, B. Liu, H. Li, W. Li, X. Qiu, N. Zhang, J. Hu, H. Pan, M. Liu, Atomically dispersed s-block magnesium sites for electroreduction of CO_2 to CO, Angew. Chem. Int. Ed. 60 (2021) 25241–25245.
[18] J. Pei, T. Wang, R. Sui, X. Zhang, D. Zhou, F. Qin, X. Zhao, Q. Liu, W. Yan, J. Dong, L. Zheng, A. Li, J. Mao, W. Zhu, W. Chen, Z. Zhuang, N-Bridged Co–N–Ni: new bimetallic sites for promoting electrochemical CO_2 reduction, Energy Environ. Sci. 14 (2021) 3019–3028.
[19] G. Shi, Y. Xie, L. Du, X. Fu, X. Chen, W. Xie, T. Lu, M. Yuan, M. Wang, Constructing Cu−C bonds in a graphdiyne-regulated Cu single-atom electrocatalyst for CO_2 reduction to CH_4, Angew. Chem. Int. Ed. 61 (2022), e202203569.
[20] Y. Zhang, Q. Zhou, Z. Qiu, X. Zhang, J. Chen, Y. Zhao, F. Gong, W. Sun, Tailoring coordination microenvironment of Cu(I) in metal–organic frameworks for enhancing electroreduction of CO_2 to CH_4, Adv. Funct. Mater. 32 (2022) 2203677.
[21] L. Han, S. Song, M. Liu, S. Yao, Z. Liang, H. Cheng, Z. Ren, W. Liu, R. Lin, G. Qi, X. Liu, Q. Wu, J. Luo, H.L. Xin, Stable and efficient single-atom Zn catalyst for CO_2 reduction to CH_4, J. Am. Chem. Soc. 142 (2020) 12563–12567.
[22] H. Yang, Y. Wu, G. Li, Q. Lin, Q. Hu, Q. Zhang, J. Liu, C. He, Scalable production of efficient single-atom copper decorated carbon membranes for CO_2 electroreduction to methanol, J. Am. Chem. Soc. 141 (2019) 12717–12723.
[23] G. Wen, B. Ren, M.G. Park, J. Yang, H. Dou, Z. Zhang, Y. Deng, Z. Bai, L. Yang, J. Gostick, G.A. Botton, Y. Hu, Z. Chen, Ternary Sn-Ti-O electrocatalyst boosts the stability and energy efficiency of CO_2 reduction, Angew. Chem. Int. Ed. 59 (2020) 12860–12867.
[24] K. Lakshmanan, W. Huang, S.A. Chala, B.W. Taklu, E.A. Moges, J. Lee, P. Huang, Y. Lee, M. Tsai, W. Su, B.J. Hwang, Highly active oxygen coordinated configuration of Fe single-atom catalyst toward electrochemical reduction of CO_2 into multi-carbon products, Adv. Funct. Mater. 32 (2022) 2109310.
[25] X. Su, Z. Jiang, J. Zhou, H. Liu, D. Zhou, H. Shang, X. Ni, Z. Peng, F. Yang, W. Chen, Z. Qi, D. Wang, Y. Wang, Complementary operando spectroscopy identification of in-situ generated metastable charge-asymmetry Cu_2-CuN_3 clusters for CO_2 reduction to ethanol, nature, Communications 13 (2022) 1322.
[26] X. Qiu, H. Zhu, J. Huang, P. Liao, X. Chen, Highly selective CO_2 electroreduction to C_2H_4 using a metal–organic framework with dual active sites, J. Am. Chem. Soc. 143 (2021) 7242–7246.
[27] R. Wang, J. Liu, Q. Huang, L. Dong, S. Li, Y. Lan, Partial coordination-perturbed Bi-copper sites for selective electroreduction of CO_2 to hydrocarbons, Angew. Chem. Int. Ed. 60 (2021) 19829–19835.
[28] H. Luo, B. Li, J.-G. Ma, P. Cheng, Surface modification of nano-Cu_2O for controlling CO_2 electrochemical reduction to ethylene and syngas, Angew. Chem. Int. Ed. 61 (2022), e202116736.
[29] W. Liu, P. Zhai, A. Li, B. Wei, K. Si, Y. Wei, X. Wang, G. Zhu, Q. Chen, X. Gu, R. Zhang, W. Zhou, Y. Gong, Electrochemical CO_2 reduction to ethylene by ultrathin CuO nanoplate arrays, Nat. Commun. 13 (2022) 1877.
[30] Y. Wang, W. Zhou, R. Jia, Y. Yu, B. Zhang, Unveiling the activity origin of a copper-based electrocatalyst for selective nitrate reduction to ammonia, Angew. Chem. Int. Ed. 59 (2020) 5350–5354.
[31] C. Clark, C. Reddy, H. Xu, K. Heck, G. Luo, T.P. Senftle, M. Wong, Mechanistic insights into pH-controlled nitrite reduction to ammonia and hydrazine over rhodium, ACS Catalysis 10 (2020) 494–509.
[32] J. Zhang, Z. Zhou, Z. Feng, H. Zhao, G. Zhao, Fast generation of hydroxyl radicals by rerouting the electron transfer pathway via constructed chemical channels during the photo-electro-reduction of oxygen, Environ. Sci. Technol. 56 (2022) 1331–1340.
[33] L. Yuan, S. Hung, Z. Tang, H. Chen, Y. Xiong, Y. Xu, Dynamic evolution of atomically dispersed cu species for CO_2 photoreduction to solar fuels, ACS, Catalysis 9 (2019) 4824–4833.
[34] G. Kresse, J. Furthmüller, Efficiency of ab-initio total energy calculations for metals and semiconductors using a plane-wave basis set, Comput. Mater. Sci. 6 (1996) 15–50.
[35] G. Kresse, J. Furthmüller, Efficient iterative schemes for ab initio total-energy calculations using a plane-wave basis set, Phys. Rev. B 54 (1996) 11169–11186.
[36] J.P. Perdew, K. Burke, M. Ernzerhof, Generalized gradient approximation made simple, Phys. Rev. Lett. 77 (1996) 3865–3868.
[37] G. Kresse, D. Joubert, From ultrasoft pseudopotentials to the projector augmented-wave method, Phys. Rev. B 59 (1999) 1758–1775.
[38] P.E. Blöchl, Projector augmented-wave method, Phys. Rev. B 50 (1994) 17953–17979.
[39] S.L. Dudarev, G.A. Botton, S.Y. Savrasov, C.J. Humphreys, A.P. Sutton, Electron-energy-loss spectra and the structural stability of nickel oxide: an LSDA+U study, Phys. Rev. B 57 (1998) 1505–1509.
[40] S. Grimme, J. Antony, S. Ehrlich, H. Krieg, A consistent and accurate ab initio parametrization of density functional dispersion correction (DFT-D) for the 94 elements H-Pu, The, J. Chem. Phys. 132 (2010).
[41] G. Henkelman, B.P. Uberuaga, H. Jónsson, A climbing image nudged elastic band method for finding saddle points and minimum energy paths, The, J. Chem. Phys. 113 (2000) 9901–9904.
[42] M. Liang, X. Li, L. Jiang, P. Ran, H. Wang, X. Chen, C. Xu, M. Tian, S. Wang, J. Zhang, T. Cui, L. Qu, Femtosecond laser mediated fabrication of micro/nanostructured TiO_{2-x} photoelectrodes: Hierarchical nanotubes array with oxygen vacancies and their photocatalysis properties, Appl. Catal. B: Environ. 277 (2020), 119231.
[43] K.I. Hadjiivanov, Identification of neutral and charged N_xO_y surface species by IR spectroscopy, Catal. Rev. 42 (2000) 71–144.
[44] H. Chen, C.E. Nanayakkara, V.H. Grassian, Titanium dioxide photocatalysis in atmospheric chemistry, Chem. Rev. 112 (2012) 5919–5948.
[45] Y. Yao, S. Zhu, H. Wang, H. Li, M. Shao, A. Spectroscopic, Study of electrochemical nitrogen and nitrate reduction on rhodium surfaces, Angew. Chem. Int. Ed. 59 (2020) 10479–10483.
[46] R. De, S. Gonglach, S. Paul, M. Haas, S.S. Sreejith, P. Gerschel, U. Apfel, T. H. Vuong, J. Rabeah, S. Roy, W. Schöfberger, Electrocatalytic reduction of CO_2 to acetic acid by a molecular manganese corrole complex, Angew. Chem. Int. Ed. 59 (2020) 10527–10534.
[47] J. Wang, H. Zhang, K. Jiang, W. Cai, From HCOOH to CO at Pd electrodes: a surface-enhanced infrared spectroscopy study, J. Am. Chem. Soc. 133 (2011) 14876–14879.
[48] C. Chen, X. Zhu, X. Wen, Y. Zhou, L. Zhou, H. Li, L. Tao, Q. Li, S. Du, T. Liu, D. Yan, C. Xie, Y. Zou, Y. Wang, R. Chen, J. Huo, Y. Li, J. Cheng, H. Su, X. Zhao, W. Cheng, Q. Liu, H. Lin, J. Luo, J. Chen, M. Dong, K. Cheng, C. Li, S. Wang, Coupling N_2 and CO_2 in H_2O to synthesize urea under ambient conditions, Nature, Nature Chem. 12 (2020) 717–724.